Support-dependent rate-determining step of CO_2 hydrogenation to formic acid on metal oxide supported Pd catalysts

Zhenhua Zhang [a], Liyuan Zhang [b], Siyu Yao [c], Xiaozhe Song [a], Weixin Huang [b], Max J. Hülsey [a,*], Ning Yan [a,*]

[a] Department of Chemical and Biomolecular Engineering, National University of Singapore, Blk E5, 4 Engineering Drive 4, Singapore 117585, Singapore
[b] Hefei National Laboratory for Physical Sciences at Microscale, CAS Key Laboratory of Materials for Energy Conversion and Department of Chemical Physics, University of Science and Technology of China, Hefei 230026, PR China
[c] Chemistry Department, Brookhaven National Laboratory, Upton, NY 11973, United States

ABSTRACT

Investigating the mechanism of CO_2 transformation into value-added chemicals is crucial for developing improved heterogeneous catalysts. In the present study, two common metal oxide (CeO_2 and ZnO) supported Pd catalysts were studied in detail. Basic sites on the support promote CO_2 activation to form surface adsorbed intermediates that further react with hydrogen atoms on metallic palladium to form formic acid. As such, both the support basicity and the (electronic) structure of Pd are critical parameters determining the catalytic performance, where the relative reaction rate for CO_2 activation and hydrogenation decides which step is rate-determining. Pd/CeO_2 with a higher density of basic sites readily activates CO_2 and therefore the hydrogenation is the limiting step governed by the nature of the Pd species on the support. For Pd/ZnO, however, the rate-determining step is the formation of adsorbed carbonaceous intermediates due to the low density of basic sites and thus, the structure of Pd has little influence on the catalytic performance. These insights are further validated on a Pd/TiO_2 catalyst, in which the optimized basic site density and Pd structure enhanced CO_2 hydrogenation activity of up to an order of magnitude.

© 2019 Elsevier Inc. All rights reserved.

1. Introduction

A net-zero fuel economy may become possible if energy from renewable resources can be employed to produce CO_2-based fuels or energy carriers such as alcohols, hydrocarbons and formic acid (FA, HCOOH) [1–9]. FA is an attractive liquid product that is easily available via CO_2 hydrogenation with H_2 [10]. CO_2 hydrogenation to FA using heterogeneous catalysts is first reported over a century ago using Pd black as a catalyst [2,11]. Since then, the synthesis of FA based on heterogeneous catalytic systems was gradually developed on various supported metal catalysts, mainly including Ru-, Au- and Pd-based catalysts [12–30], among which Pd received most attention [17–22,26–28,31].

Stalder et al. studied the catalytic efficiency of Pd supported on various supports ($BaSO_4$, γ-Al_2O_3 and carbon) and observed that Pd/C showed the highest activity (25 h^{-1}) [17]. Similarly, Su et al. observed that Pd/AC exhibited superior performance with TOFs of 527 h^{-1} using $NaHCO_3$ as reagent and 1103 h^{-1} using NH_4HCO_3

as reagent [18]. Li et al. used heterogeneous Pd catalyst supported on mesoporous graphitic carbon nitride for catalytic hydrogenation reaction and demonstrated that the high TOF (144 h^{-1}) resulted from the synergetic effect between the basic sites of mpg-C_3N_4 support and reduced Pd nanoparticles (NPs), as suggested by DFT modelling [21]. Besides those advances of carbon-based supported Pd catalysts, the use of metal oxides remains underexplored despite their high stability and versatility in terms of redox and acid-base properties. Although it has been proposed that the catalytic activity is closely related to the choice of the metal oxide support, the governing factors such as the density and strength of basic sites has not been systematically investigated.

As an essential part of the commercial methanol synthesis catalyst, ZnO is the most widely investigated metal oxide support for CO_2 hydrogenation and is believed to contribute to the catalytic reaction in a variety of ways. In particular, a Pd/ZnO catalyst was previous shown to be active in converting CO_2 into methanol in which the PdZn alloy particles were assigned as active species [32]. Among other metal oxides, ZrO_2, In_2O_3 and mixed metal oxides received considerable attention for methanol synthesis [33,34]. For the CO_2 hydrogenation to FA, metal oxide supports like Al_2O_3, MgO, CeO_2 or ZnO and other basic supports like $BaSO_4$ and $CaCO_3$

all show performance inferior to the above-mentioned carbon-supported catalysts [17,18,22,35–38]. Those previous reports did not discuss in detail the reason for this activity difference and thus do not provide reasonable design strategies regarding the development of enhanced metal oxide-supported catalysts.

By comparing the catalytic activity, structure and mechanism of Pd catalysts supported on CeO_2 and ZnO with different weight loadings, we have identified the main structural features governing the CO_2 hydrogenation activity. The Pd particle size and electronic structure was found to deviate between the two different supports, but the electronic state of the metal only affected FA formation on CeO_2 but not on ZnO. A thorough kinetic and in situ DRIFT spectroscopic analysis reveal that the rate-limiting step is different for the two catalysts, offering guidance to develop a TiO_2-supported Pd catalyst with superior activity to produce FA from CO_2 under mild reaction conditions.

2. Experimental

All chemicals were purchased from Sigma-Aldrich and used without further purification. Pd/CeO_2 catalysts with varied Pd loadings were synthesized by a co-precipitation method. Typically, an aqueous solution of 1 mol L^{-1} Na_2CO_3 was added dropwise to an aqueous mixture (100 mL) of $PdCl_2$ with different contents and cerium (III) nitrate hexahydrate (5 g L^{-1}) at 323 K until the pH value reached 10 with the stirring rate of 600 r/min. Then, the mixed solution was kept for 3 h under continuous stirring. The resulting precipitate was acquired by centrifugation, and then washed with deionized water until no Cl^- can be detected. The acquired solids were dried in an oven at 333 K for 12 h, then calcined in air at 623 K for 2 h, and eventually reduced in 5% H_2/N_2 with a flow rate of 30 mL min^{-1} at 473 K for 1 h. The volumes of added $PdCl_2$ aqueous solution was used to change the amounts of added $PdCl_2$. The acquired catalysts were denoted as $x\%Pd/CeO_2$ (x is the calculated Pd:CeO_2 weight ratios). Pd/ZnO and Pd/TiO_2 catalyts were prepared following a similar procedure and the details are provided in the supporting information.

The reaction was conducted in a high-pressure batch reactor. Sodium bicarbonate was employed as the carbon source. In a typical procedure, sodium bicarbonate (168 mg, 2 mmol) dissolved in H_2O (2 mL) and catalyst (10–20 mg) were added into the reactor (10 mL). After purging N_2 3 times, the reactor was charged with H_2 (2 MPa) and sealed. The reactor was then placed in a preheated oil bath and at 800 r/min stirring rate. After 1 h, the reaction was quenched by placing the reactor in cold water. The products were analysed by high performance liquid chromatography (HPLC, SHIMADZU, Singapore) equipped with a Hi-plex H column and RID detector. For recycling tests, the spent catalysts were washed by deionized water and dried overnight in an oven at 333 K before using for the next batch reaction. Further details on kinetic study are provided in the supporting information. For the CO_2 hydrogenation experiments, 10 mg catalyst was used in a solution of 2 mL 1.0 mol/L base (NaOH, KOH or NEt_3). The reactor was then pressurized with 14 bar gas mixture of 50 vol% H_2 and 50 vol% CO_2. After stirring for 1 h at room temperature, the mixture was filtered and analysed. Analysis of the product gas mixtures was performed using gas phase FTIR on a Nicolet iS50 FT-IR spectrometer with a CaF_2-fitted FTIR cell. Before measurements, the cell was evacuated, the background was collected and then the respective gas mixture was allowed to fill the FTIR cell upon which the mixture was analysed.

TOFs have been calculated as follows:

$$TOF = \frac{moles\ of\ formate\ generated}{moles\ of\ surface\ Pd\ on\ the\ catalyst\ *\ time}$$

The amount of surface Pd was calculated as following using the following simple equation adopted from the literature [39]:

$$Pd_{surface} = Pd_{total} * Dispersion = \frac{Pd_{total}}{d(average\ size)}$$

Instrument and analysis details for inductively coupled plasma optical emission spectrometer (ICP-OES), X-ray diffraction (XRD), X-ray photoelectron spectroscopy (XPS), transmission electron microscopy (TEM) and high-resolution transmission electron microscopy (HRTEM), X-ray absorption spectroscopy (XAS), H_2-temperature programmed reduction (H_2-TPR) and CO_2-temperature programmed desorption (CO_2-TPD), in situ diffuse reflectance infrared Fourier transformed spectra (DRIFTS) are provided in the supporting information.

3. Results and discussion

A series of Pd/CeO_2 and Pd/ZnO catalysts with 0.05, 0.1, 0.2 and 2 wt% Pd loadings were synthesized by co-precipitation. As measured by ICP-OES (data summarized in Table S1), the actual Pd contents are close to the amount of added Pd precursor during synthesis, indicating that Pd was completely precipitated onto the supports. The XRD patterns (Fig. S1) of the supported Pd catalysts only show diffraction patterns arising from the metal oxides, except for a weak reflection from the Pd{1 1 1} crystal face observed on 2%Pd/ZnO catalyst. Fig. 1 shows the TEM images of $0.05\%Pd/CeO_2$, $2\%Pd/CeO_2$, 0.05%Pd/ZnO, and 2%Pd/ZnO catalysts. Pd NPs were absent on both $0.05\%Pd/CeO_2$ and 0.05%Pd/ZnO, indicating that Pd is highly dispersed. However, Pd NPs were easily identified on $2\%Pd/CeO_2$ and 2%Pd/ZnO, with size distributions of 3.4 ± 0.8 nm (Fig. S2) and 5.4 ± 1.4 nm (Fig. S3), respectively. Their corresponding HRTEM images reveal a lattice fringe of 2.2 Å of these particles, which matches well with the spacing of Pd{1 1 1} crystal plane, demonstrating that Pd exists in metallic form. The electronic and coordination structures of Pd in various catalysts were determined by XAS. In the Pd L_{III}-edge XANES spectra (Fig. 2A1), the adsorption edges of Pd on ZnO and CeO_2 are almost identical at 2 wt% Pd loading, close to metallic Pd. However, the absorption edge shifts to higher energy when Pd loading is decreased to 0.05%, suggesting that Pd species are in the oxidized form. The shift on $0.05\%Pd/CeO_2$ is more than that on 0.05%Pd/ZnO, indicating that Pd is more positively charged on CeO_2. Their corresponding Pd L_{III}-edge EXAFS spectra show Pd-Pd and Pd-O scattering contributions on $2\%Pd/CeO_2$ and 2%Pd/ZnO, whereas only Pd-O scattering is observed for $0.05\%Pd/CeO_2$ and 0.05%Pd/ZnO catalysts (Fig. 2A2).

The Pd $3d_{5/2}$ XPS spectra (Fig. 2B1 and B2) exhibit one symmetric component with binding energy of 337.6 eV on $0.05\%Pd/CeO_2$ and $0.1\%Pd/CeO_2$ catalysts and binding energy of 336.4 eV on 0.05%Pd/ZnO catalyst, respectively. These Pd $3d_{5/2}$ binding energies typically arise from Pd(II) features, assignable to highly-dispersed Pd interacting with surface O on the supports [40]. It is well-known that supports have an influence on the electronic structure of supported Pd, thus the similar Pd(II) features exhibit different binding energies on Pd/CeO_2 and Pd/ZnO catalysts [41,42]. Besides the Pd(II) features, another component with the Pd $3d_{5/2}$ binding energy at 335.4–335.6 eV belonging to Pd(0) appears on higher loading Pd/CeO_2 and Pd/ZnO catalysts, fully consistent with XAS and TEM findings. In Ce 3d and Zn 2p XPS spectra (Fig. S4), only Zn(II) features appear on all Pd/ZnO catalysts while a weak Ce(III) feature, in addition to the dominant Ce(IV) features, is present on (0.2% or 2%) Pd/CeO_2 catalysts, indicating that higher Pd loading on CeO_2 is beneficial for the reduction of Ce^{4+} due to Pd-CeO_2 interaction.
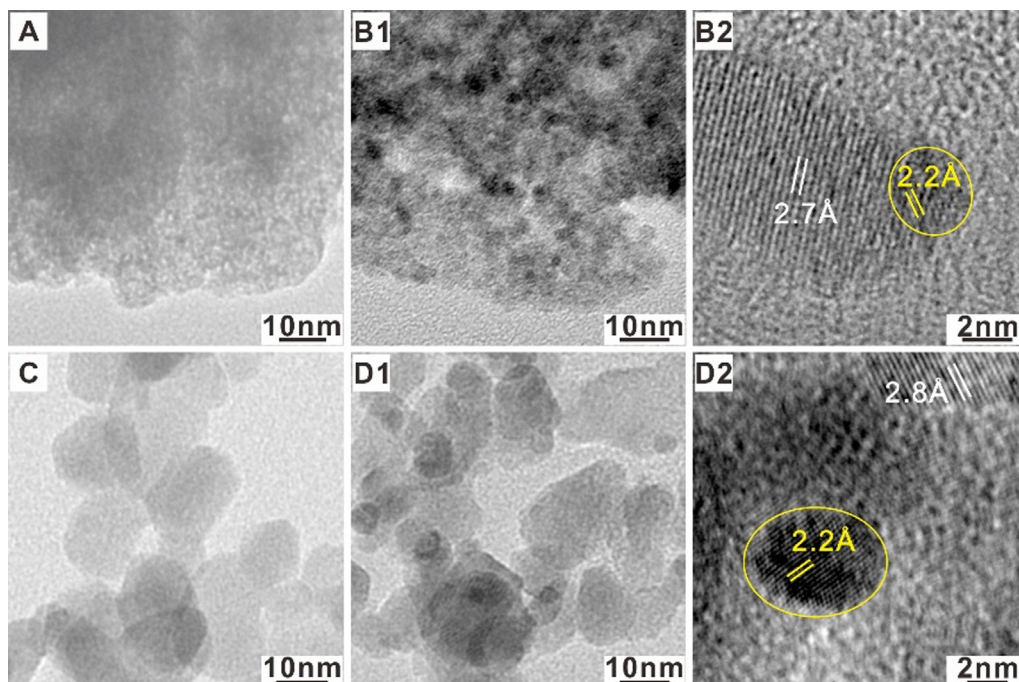
Fig. 1. TEM images of (A) 0.05% Pd/CeO$_2$ and (C) 0.05% Pd/ZnO; TEM and HRTEM images of (B1, B2) 2% Pd/CeO$_2$ and (D1, D2) 2% Pd/ZnO. The lattice fringes (indicated in yellow and white) of 2.7, 2.8, and 2.2 Å, correspond to the spacing of CeO$_2$\{2 0 0\} (JCPDS card number 43-1002), ZnO\{1 0 0\} (JCPDS card number 89-1397), and Pd\{1 1 1\} (JCPDS card number 65-2867) crystal planes, respectively.
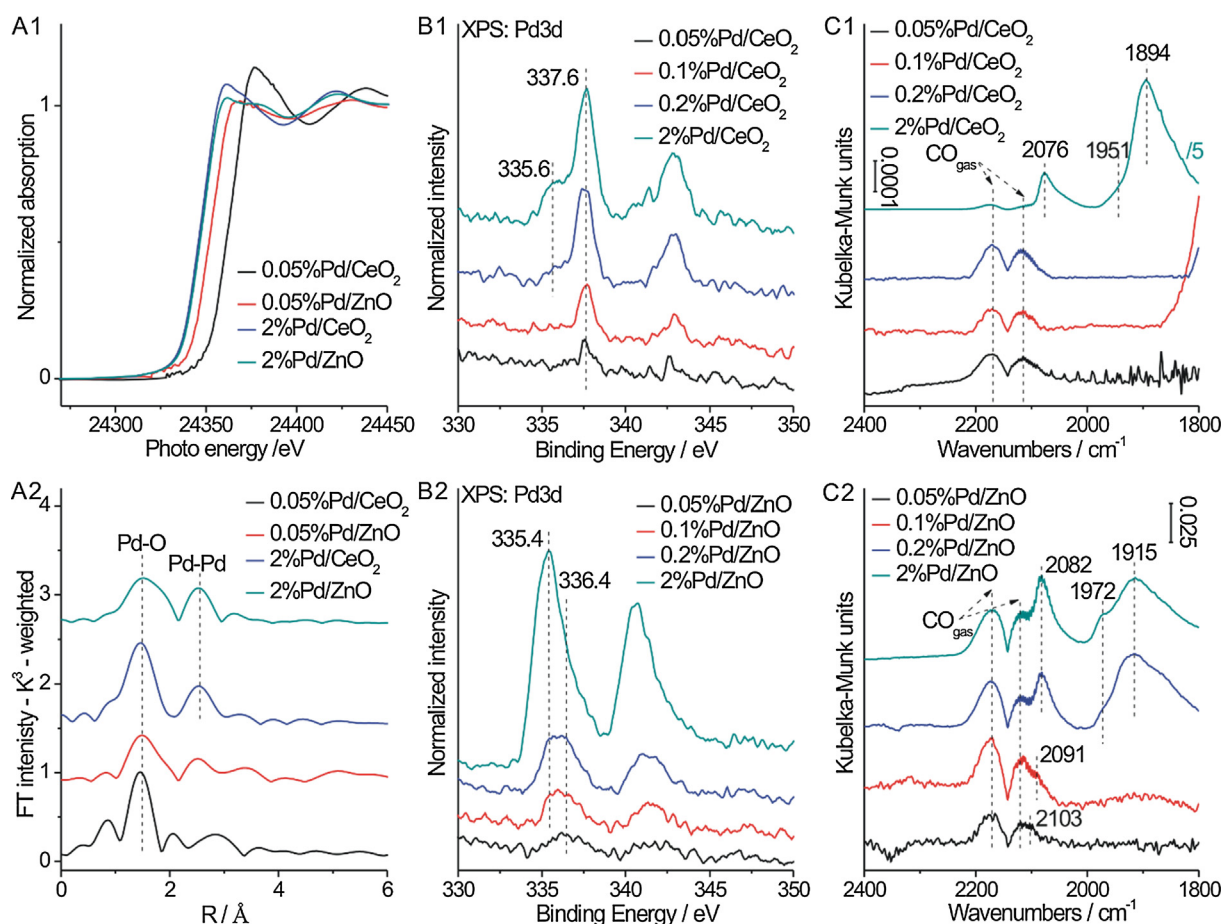

Fig. 2. (A1) Pd L$_{III}$-edge XANES spectra and (A2) Pd L$_{III}$-edge EXAFS spectra of various Pd-based catalysts; Pd 3d XPS spectra of various Pd loadings of (B1) Pd/CeO$_2$ and (B2) Pd/ZnO catalysts; *In situ* DRIFTS spectra of CO adsorbed at 298 K on various Pd loadings of (C1) Pd/CeO$_2$ and (C2) Pd/ZnO catalysts.

In the CO adsorption DRIFT spectra (Fig. 2C1 and C2), absorption peaks at 2082, 1982, and 1915 cm^{-1} are observed, which are commonly assigned to linearly or bridged adsorbed CO or CO on 3-fold Pd^0 sites [43]. All those signals are present on 0.2%Pd/ZnO and 2% Pd/ZnO catalysts. However, when the Pd loading is decreased to 0.1%, linear adsorption of CO shifts to 2091 cm^{-1} accompanied by significantly weakened bridged/3-fold adsorption of CO, suggesting the presence of positively charged Pd species [44]. When Pd loading is further reduced to 0.05%, a further blue shift of the linearly adsorbed CO to 2103 cm^{-1} is observed [44]. On 2%Pd/CeO$_2$, all above-mentioned metallic Pd-bound CO signals are present, but such features disappear on samples with lower Pd loadings. Based on TEM, XRD, XAS, XPS and CO-DRIFT-IR studies, we conclude that Pd predominantly stays in the form of NPs on CeO$_2$ and ZnO at 2 wt %. As the loading decreases, the size of the NPs decreases while the percentage of charged Pd species increases. At 0.05 wt%, Pd stays almost exclusively as atomically dispersed species with a valence state close to + 2.

The catalytic performance of various Pd/CeO$_2$ and Pd/ZnO catalysts was evaluated in the hydrogenation of NaHCO$_3$ into formate at 373 K. Total Pd amounts were used to determine the production rate of formate. Interestingly, the rates exhibit opposite variation trends as a function of Pd loading on CeO$_2$ and ZnO (Fig. 3A). For Pd/CeO$_2$ catalysts, the production rate slightly increases when the Pd loading is increased from 0.05% to 0.2%, and further increases significantly on 2%Pd/CeO$_2$. In contrast, the production rate gradually decreases on Pd/ZnO catalysts with increasing Pd loading. To better understand the structure–activity correlations, Pd catalysts on CeO$_2$ and ZnO supports with two extreme loadings, i.e., 0.05 wt% and 2 wt%, were selected for a more detailed study.

The TOF values were obtained for Pd catalysts at 0.05% loading, assuming all Pd species are active sites since Pd is atomically dispersed. For 2 wt% catalysts, the Pd surface fraction is estimated based on the average particle size in TEM analysis (Fig. S2 and Fig. S3). The obtained TOF values revealed a remarkable difference between the CeO$_2$ and the ZnO supports (Fig. 3B). 2%Pd/CeO$_2$
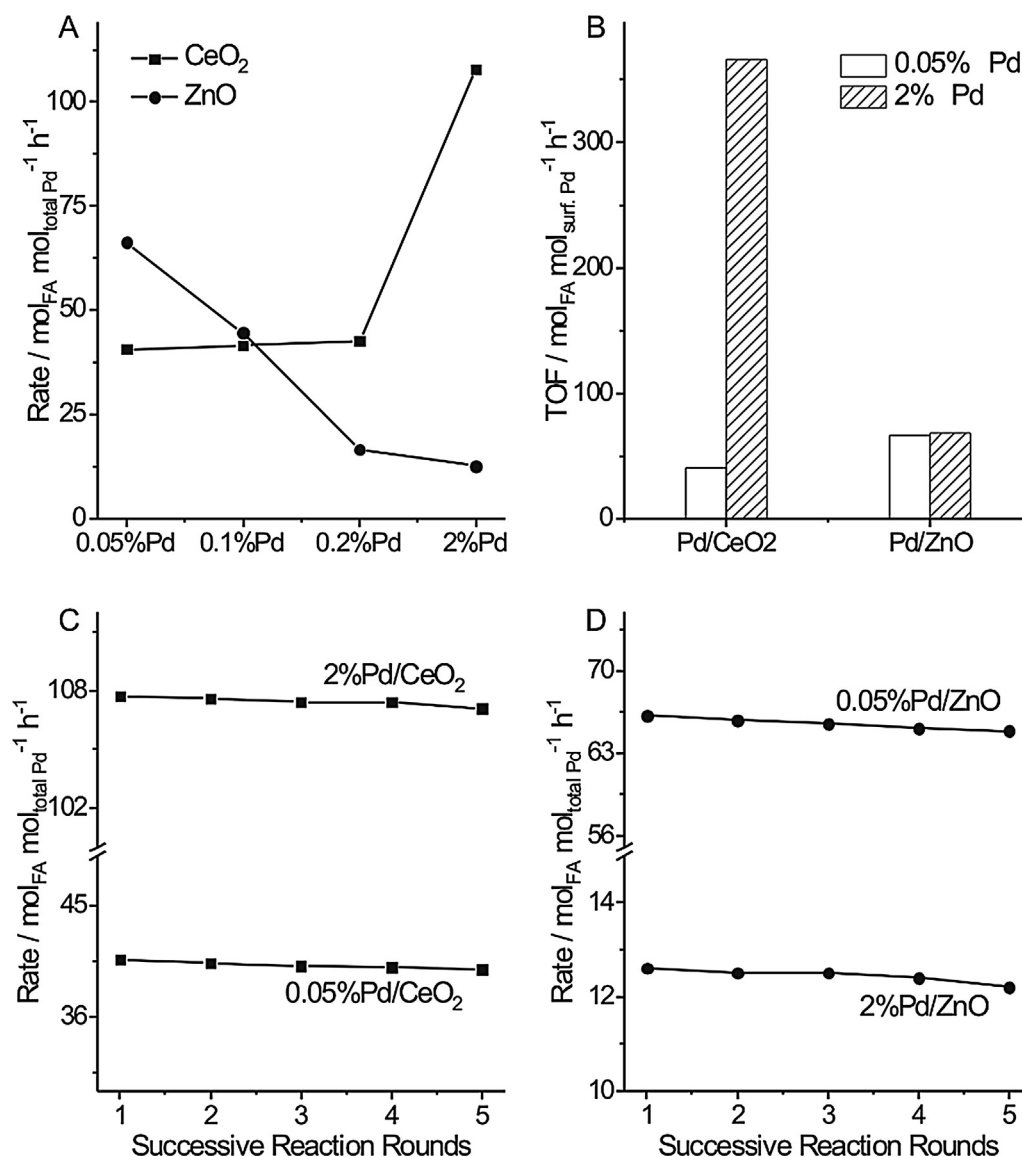

Fig. 3. (A) Formation rate of FA (mol$_{FA}$ mol$_{total\ Pd}^{-1}$h^{-1}) calculated by total Pd atoms on various Pd loadings of Pd/CeO$_2$ and Pd/ZnO catalysts at 373 K; (B) TOFs (mol$_{FA}$ mol$_{surf.\ Pd}^{-1}$h^{-1}, TOF) of FA calculated by surface Pd atoms on 0.05%Pd/CeO$_2$, 2%Pd/CeO$_2$, 0.05%Pd/ZnO, and 2%Pd/ZnO catalysts at 373 K; Reaction rate (mol$_{FA}$ mol$_{total\ Pd}^{-1}$h^{-1}) for the formation of FA on (C) 0.05Pd/CeO$_2$ and 2%Pd/CeO$_2$, and (D) 0.05Pd/ZnO and 2%Pd/ZnO over the course of five rounds of successive reaction at 373 K.

($366 \, h^{-1}$) exhibit 9 times higher TOF than $0.05\%Pd/CeO_2$ ($41 \, h^{-1}$), while the TOF numbers are identical on $2\%Pd/ZnO$ and $0.05\%Pd/ZnO$ ($\approx 68 \, h^{-1}$ vs. $\approx 66 \, h^{-1}$). These results clearly demonstrate that formate synthesis on Pd/CeO_2 is a structure sensitive reaction, where the geometry and electronic structure of Pd strongly affect catalytic activity, whereas the same reaction on Pd/ZnO catalysts is structure insensitive. Recycling experiments were conducted using the four catalysts to determine the catalyst stability (Fig. 3D). The catalytic performance is almost unchanged after 5 cycles, indicating that the structure and catalytic activity of Pd were well maintained after the reaction. In addition to sodium bicarbonate, we also used CO_2 as carbon source for hydrogenation reactions. For the aqueous phase CO_2 hydrogenation into formate, basic solutions are crucial. Both KOH and NaOH seem to benefit the CO_2 hydrogenation reaction whereas the use of NEt_3 does not yield any product (Fig. S5). Based on gas cell FTIR measurements, the mixtures of the gas after reaction do not contain significant amounts of CO and CH_4 (Fig. S6). Furthermore, no formaldehyde was observed by HPLC. Therefore, we confirm that the CO_2 hydrogenation reaction yields formate as the sole product in the system.

The calculated apparent activation energies (E_a) of CO_2 hydrogenation to FA on various Pd/CeO_2 and Pd/ZnO catalysts were determined using Arrhenius plots. Before measurements, it has been confirmed that no thermodynamic equilibrium or mass transfer limitations exist in the system (Fig. S7). For Pd/CeO_2 catalysts (Fig. 4A and Fig. S8 A&B), the calculated E_a using $0.05\%Pd/CeO_2$ and $2\%Pd/CeO_2$ catalysts were 43.5 ± 2.2 and 23.3 ± 0.2 kJ/mol, respectively, while similar E_a values of around 34 kJ/mol were obtained on $0.05\%Pd/ZnO$ and $2\%Pd/ZnO$ catalysts (Fig. 4D and Fig. S8C and D). These results further confirm that the structure of Pd strongly influences the catalytic performance of Pd/CeO_2 catalysts but does not affect activity on Pd/ZnO catalysts. Kinetic investigations indicate that the reaction orders of H_2 and sodium bicarbonate are independent on the structure of Pd species but highly dependent on the nature of the support (Fig. 4 B and C, Fig. 4 E and F, Fig. S9, and Fig. S10). Regardless of Pd loading, the reaction order of sodium bicarbonate is around 1.4 on Pd/ZnO catalysts, much higher than that on Pd/CeO_2 catalysts (around 0.6). The reaction order above 1 occurs because of the participation of bicarbonate in more than one kinetically relevant steps. On the contrary, the reaction order of H_2 is always considerably higher on Pd/CeO_2 catalysts (around 0.36–0.43) than those on Pd/ZnO catalysts (around 0.12–0.17). This finding suggests that the rate-determining step of CO_2 hydrogenation into FA is different on the two supports: bicarbonate species are involved in the rate-limiting step on ZnO-based catalysts while H_2 is more kinetically relevant on CeO_2-based catalysts.
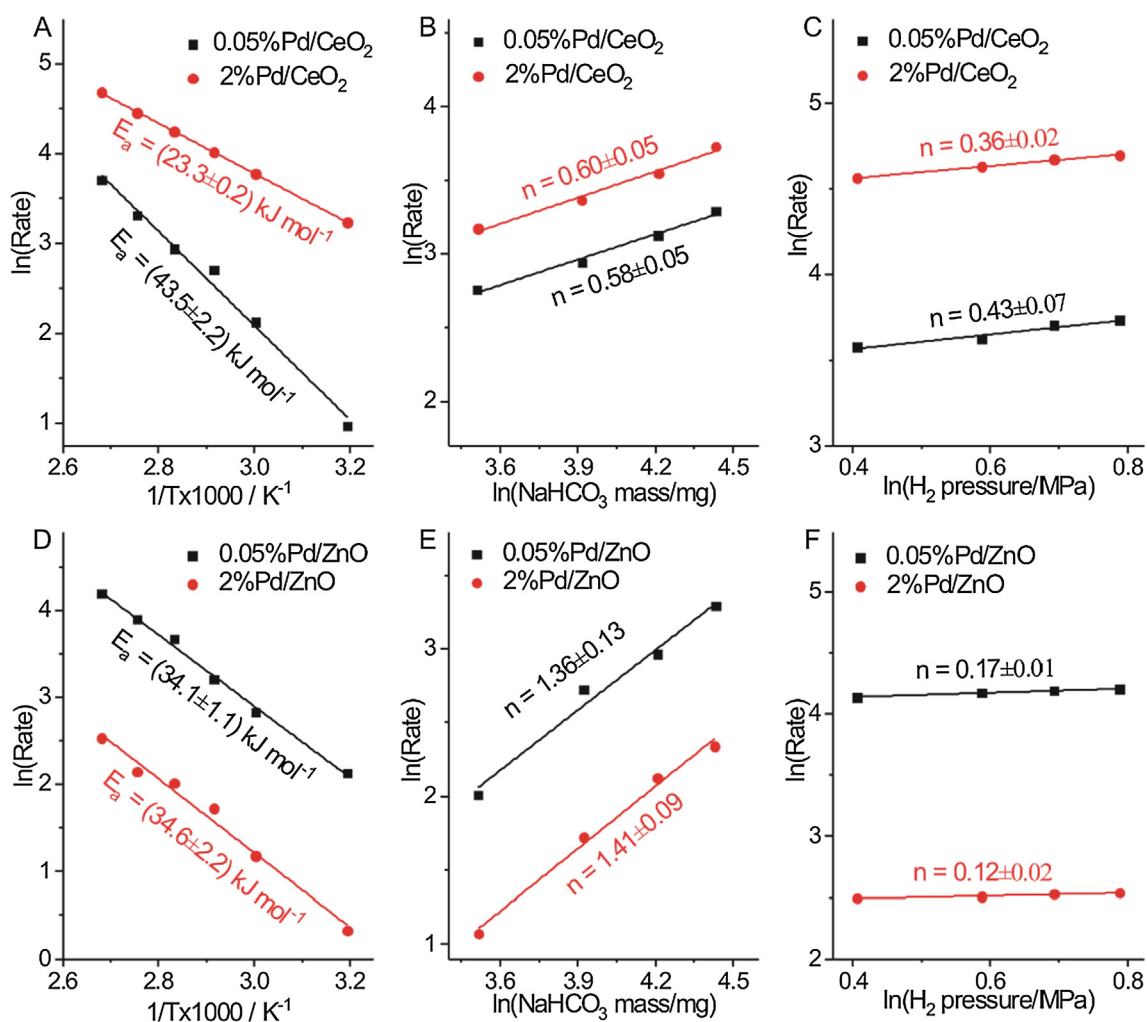
Fig. 4. Arrhenius plots of (A) $0.05\%Pd/CeO_2$ and $2\%Pd/CeO_2$ catalysts, and (D) $0.05\%Pd/ZnO$ and $2\%Pd/ZnO$ catalysts; CO_2 reaction orders of (B) $0.05\%Pd/CeO_2$ and $2\%Pd/CeO_2$ catalysts, and (E) $0.05\%Pd/ZnO$ and $2\%Pd/ZnO$ catalysts at 373 K; H_2 reaction orders of (C) $0.05\%Pd/CeO_2$ and $2\%Pd/CeO_2$ catalysts, and (F) $0.05\%Pd/ZnO$ and $2\%Pd/ZnO$ catalysts at 373 K.

In situ DRIFTS was used to systematically study the reaction mechanism for FA synthesis by CO_2 hydrogenation on Pd/CeO_2 and Pd/ZnO. Band assignments for all different vibrations observed by *in situ* DRIFTS are summarized in Table 1 [45–49]. All catalysts were first activated by pure H_2 at 373 K for 1 h, after which the reaction cell was purged with high purity N_2 before pure CO_2 was introduced at the same temperature (see Fig. 5). Bidentate carbonate (1680–1682 cm^{-1}) and bicarbonate (1240–1276 and 1630–1638 cm^{-1}) were immediately generated on the two Pd/CeO_2 catalysts reaching saturation level within 1 min, while much slower generation of adsorbed bidentate carbonate (1668 cm^{-1}), bicarbonate (1231, 1443–1446, and 1616–1617 cm^{-1}), and bidentate formate (1379–1380 and 1563–1564 cm^{-1}) species were observed on Pd/ZnO catalysts. In fact, these species did not reach saturation level even after 1 h. It is well-known that certain metal oxides bind and potentially activate CO_2 on their surface [50,51]. Thus, these results suggest that the reaction of CO_2 with ZnO to form surface adsorbed carbonaceous species is more difficult compared to CeO_2, in accordance with the higher reaction order of bicarbonate on Pd/ZnO catalysts. After

exposure under CO_2 for 1 h, the reaction cell was purged by high purity N_2 again. The intensity of the bands by formed carbonaceous species had no appreciable change on Pd/CeO_2 catalysts, indicating these surface species do not undergo desorption under applied condition (Fig. S13). Next, pure H_2 was introduced into the *in situ* cell to probe the reaction between H_2 and the pre-formed carbonaceous species on the surface. The bands at 1243–1279, 1632–1639, 1675–1678, and 3300–3410 cm^{-1} decrease slowly on Pd/CeO_2 catalysts, where the bands vanish faster at a higher Pd loading in agreement with the fact the $2\%Pd/CeO_2$ has higher activity than $0.05\%Pd/CeO_2$. In sharp contrast, bands for surface adsorbed carbonaceous species on Pd/ZnO vanish almost immediately on both 0.05% and 2.0% Pd/ZnO catalysts. These results provide evidence that the formation of bicarbonate species is the rate-determining step on Pd/ZnO. In contrast, reaction of H with surface carbonaceous species is slow on Pd/CeO_2, thus perhaps is rate-determining. Fig. 6 shows *in situ* DRIFT spectra under an atmosphere of CO_2 and H_2 (1:1) on typical Pd/CeO_2 and Pd/ZnO catalysts. Bicarbonate (1680 cm^{-1}) and bidentate carbonate (1240 and 1638 cm^{-1}) are simultaneously generated on $0.05\%Pd/CeO_2$,
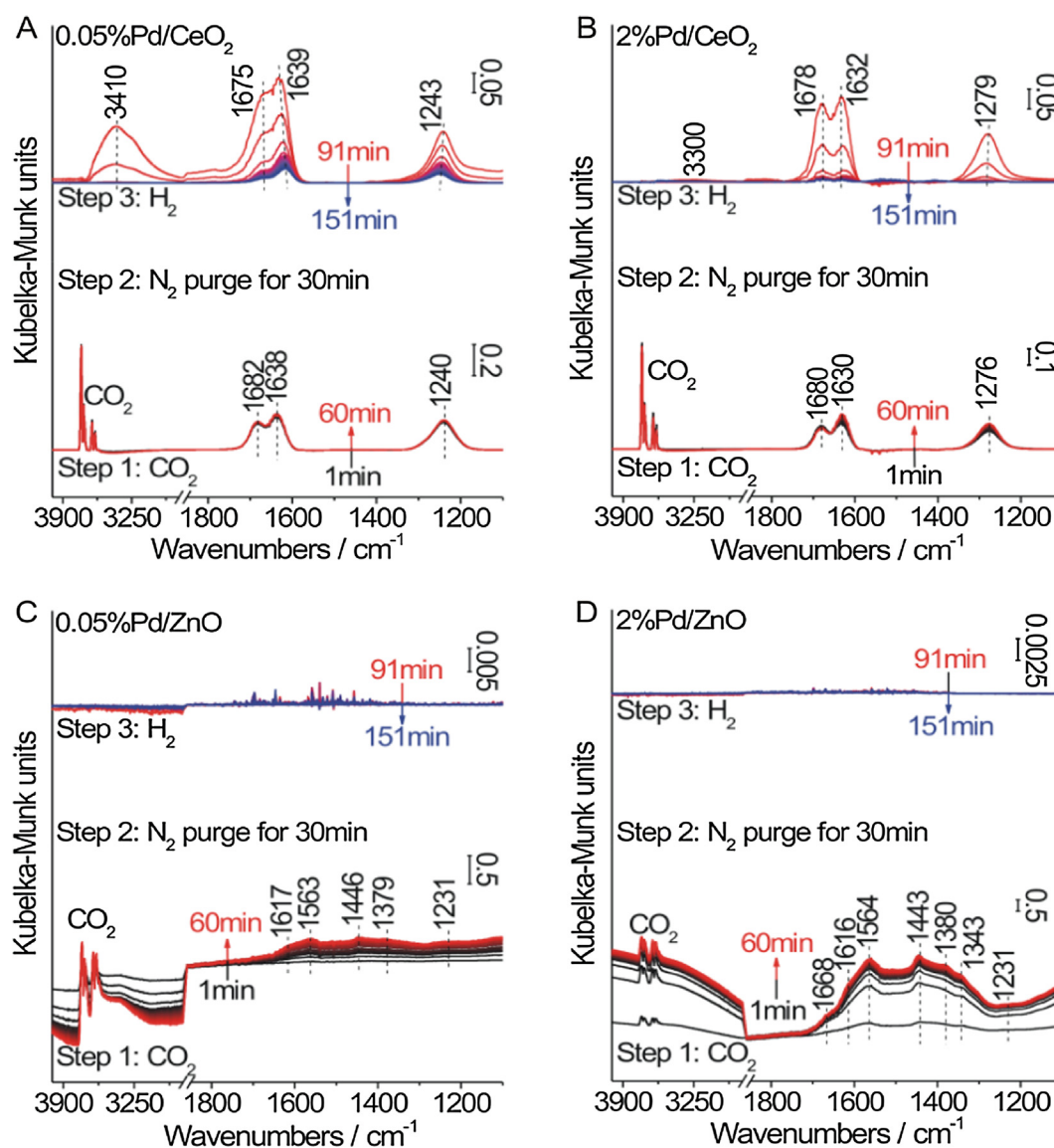

Fig. 5. *In situ* time-resolved DRIFTS spectra of first CO_2 and then H_2 stepwise reactions at 373 K on (A) $0.05\%Pd/CeO_2$, (B) $2\%Pd/CeO_2$, (C) $0.05\%Pd/ZnO$, and (D) $2\%Pd/ZnO$ catalysts after pretreatment by H_2 at 373 K for 1 h.

Table 1
Assignment of vibrational bands in the DRIFTS spectra of surface species at various supported Pd catalysts.

Assignment	Schematic structure	Bands (cm^{-1})				Ref.
		0.05% Pd/CeO$_2$	2% Pd/CeO$_2$	0.05% Pd/ZnO	2% Pd/ZnO	
Bidentate carbonate		1665 ∼ 1682	1678 ∼ 1680	–	1668	26
Bicarbonate		1240 ∼ 1256	1616 ∼ 1632	1231 ∼ 1250	1231 ∼ 1238	26,27
		1615 ∼ 1639	1263 ∼ 1279	1442 ∼ 1446	1442 ∼ 1443	
				1615 ∼ 1630	1616 ∼ 1645	
Bidentate formate		–	–	1379 ∼ 1395	1380 ∼ 1396	28
				1563 ∼ 1567	1564 ∼ 1565	
Monodentate carbonate		–	1401 ∼ 1409	–	–	29
			1523 ∼ 1540			
Polydentate carbonate		1489	–	–	–	28
Unassigned carbonate		–	–	1338 ∼ 1341	1340 ∼ 1344	28
Hydroxyl groups		3300 ∼ 3500				29,30
CO$_2$(g) and CO$_2$(a)		3550 ∼ 3750				30
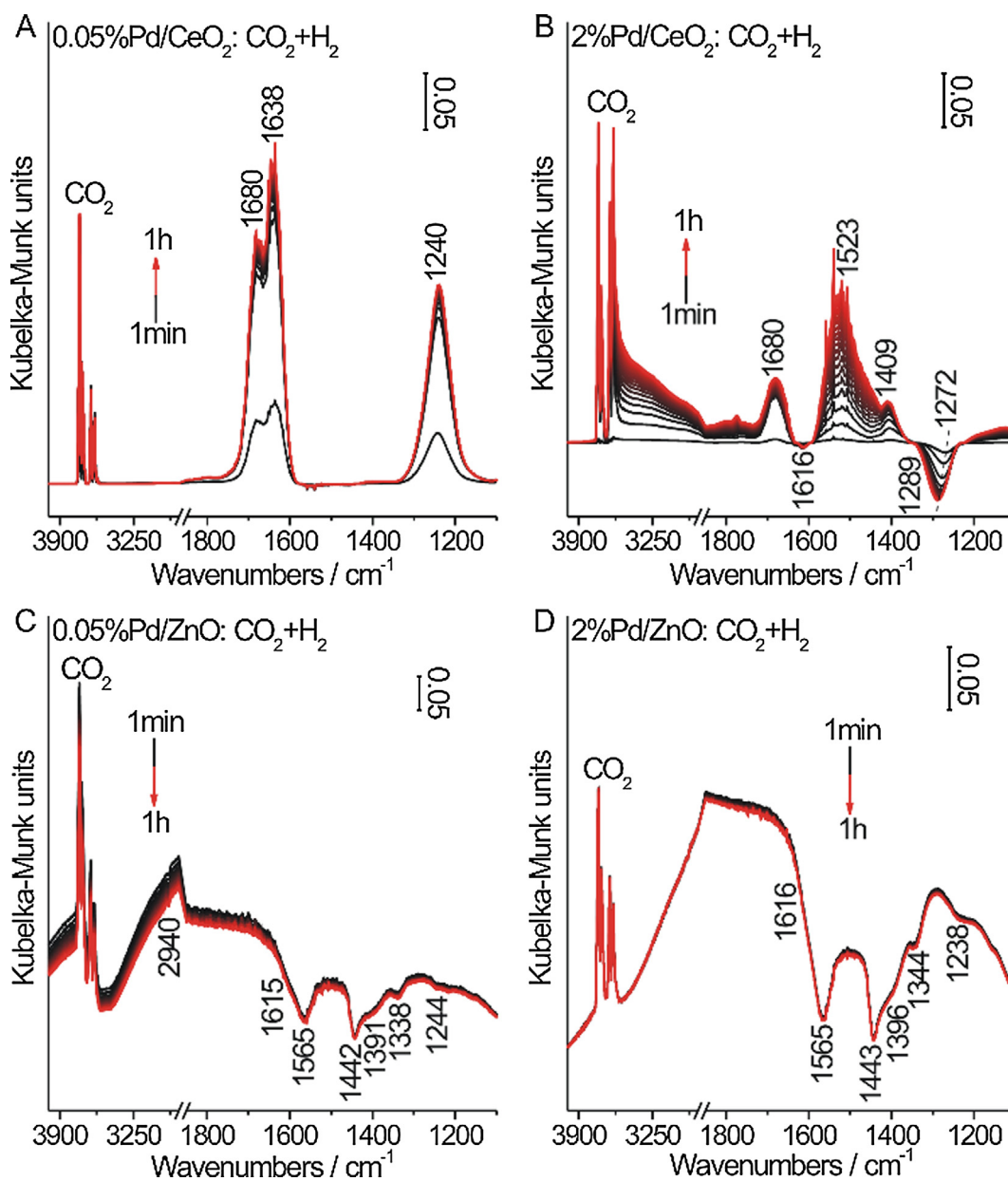
Fig. 6. *In situ* DRIFT spectra of CO$_2$ hydrogenation reaction under an atmosphere of CO$_2$ and H$_2$ (1:1) on (A) 0.05%Pd/CeO$_2$, (B) 2%Pd/CeO$_2$, (C) 0.05%Pd/ZnO, and (D) 2%Pd/ZnO catalysts at 373 K.

but only bicarbonate (1272–1289 and 1616 cm^{-1}) significantly decreases on 2%Pd/CeO$_2$. This bicarbonate species is generated simultaneously with bidentate carbonate during CO_2 activation, but disappears rapidly in $CO_2 + H_2$ atmosphere on high-performance catalyst, indicating that bicarbonate is the active intermediate for CO_2 hydrogenation to FA. Moreover, according to the schematic structure in Table 1, we propose that bicarbonate can be formed by bidentate carbonate reacting with atomic H. For various Pd/ZnO catalysts, both catalysts exhibit significant negative peaks of bicarbonate (1238–1244, 1442–1443, and 1615–1616 cm^{-1}), bidentate formate (1391–1396 and 1565 cm^{-1}), and unassigned carbonate (1338–1344 cm^{-1}). Fig. 6 provides important information concerning the Pd catalysts under working state: Pd/CeO$_2$ catalyst surface is covered with bicarbonate and bidentate carbonate, while Pd/ZnO catalyst surface has no such coverage due to faster reaction of these species than their generation. This further confirms a rapid reaction between surface carbonaceous species and atomic H on Pd/ZnO catalysts.

According to in situ DRIFTS results, we propose that surface adsorbed bicarbonate is the active intermediate for CO_2 hydrogenation to FA. It is formed by CO_2 reacting with the supports to obtain bidentate carbonate, followed by H transfer to form a bicarbonate. Reaction between adsorbed bicarbonate and activated H generates formate as the desired product. The formation of surface bicarbonate is facilitated by the support, whereas the last step is promoted by Pd. On Pd/CeO$_2$ catalyst, surface adsorbed bicarbonate is easily generated, while its reaction with atomic H is slower. Since Pd catalysed hydrogenation of surface bicarbonate is rate-determining, the structure of Pd species on CeO$_2$ decides the catalytic activity. On Pd/ZnO, CO_2 reacts with ZnO much more slowly compared to the subsequent hydrogenation steps indicating that the activation of CO_2 becomes critical. As a result, Pd/ZnO catalysts with different Pd weight loadings exhibit similar E_a and their reaction order towards bicarbonate is high. The structure of Pd has no influence on their catalytic performance since Pd does not participate in the rate-determining step.

The basicity of CeO$_2$ and ZnO were tested using CO_2-temperature programmed desorption (CO_2-TPD) measurements (Fig. 7A). The results show that the desorption temperature of CO_2 is similar for both CeO$_2$ and ZnO, starting at 315 K. However, the amount of adsorbed CO_2 is more than five times higher on CeO$_2$ compared to ZnO, indicating that CeO$_2$ has a larger number of basic sites with similar strengths. We also determined the BET surface areas for pure CeO$_2$ and ZnO to be 27.4 and 42.2 m^2/g which then allows us to estimate the density of basic sites to be 38.0 and

5.4 $\mu mol/m^2$, respectively. The same holds true for supported Pd catalysts (Fig. S14). Therefore, it can be assumed that the formation of bicarbonate is hindered by the limited density of basic sites on ZnO, resulting in the reaction of CO_2 with the basic sites on the support as rate-limiting step for CO_2 hydrogenation.

H_2-TPR experiments were conducted to investigate the reduction properties of calcined Pd/CeO$_2$, Pd/ZnO, and their corresponding supports with H_2 (Fig. 7 B&C). For individual supports, CeO$_2$ shows several small and broad reduction peaks around 495–740 K, which can be ascribed to the reduction of surface-capping oxygen of ceria [52]. However, no reduction peak was observed for ZnO. It has been reported that supported Pd materials can remarkably promote the reduction properties of supports [47]. This phenomenon was indeed observed on various Pd/CeO$_2$ catalysts. Three types of reduction peaks, denoted as α, β, and λ, which can be ascribed to the reduction of surface-capping oxygen of ceria, the reduction of PdO-CeO$_2$ interface, and the two-step reduction of PdO, appeared on various Pd/CeO$_2$ catalysts [52,53]. Among them, only one peak for the reduction of PdO-CeO$_2$ interface appears on (0.05%, 0.1%, or 0.2%) Pd/CeO$_2$ catalysts, while the two-step reduction of PdO only appears on 2%Pd/CeO$_2$, indicating that Pd is highly dispersed in the former three, consistent with earlier spectroscopic characterizations. On the other hand, the promotional effect of support by Pd cannot be observed on ZnO-based catalysts due to the low reducibility of ZnO. For 0.05%Pd/ZnO, no reduction peak was observed. When Pd loading increases, a broad reduction peak accompanying with a weak shoulder peak (denoted as λ), which can be ascribed to the two-step reduction of PdO [53], appears on 0.1%Pd/ZnO and 0.2% Pd/ZnO catalysts, indicating that the particle size of Pd starts to increase. An intense negative peak was observed on 2% Pd/ZnO catalyst, which is generally attributed to the decomposition of PdH phases [54]. The formation of PdH phase comes from the reduction of PdO species at ambient temperature under the reducing environment, followed by the subsequent decomposition of at higher temperature releasing hydrogen. Of note, the reduction temperature of the PdO-CeO$_2$ interface decreases with the increase of Pd loading, demonstrating that H_2 dissociation and the reaction of hydrogen atoms with CeO$_2$ occurs more easily on these samples.

Based on the above investigations, we conclude that a high-performance Pd-based catalyst for FA formation must contain two elements: enough basic sites with suitable basicity for CO_2 activation and metallic Pd species for hydrogen splitting. It has been reported that TiO$_2$ exhibits a much higher number of basic sites than CeO$_2$ [55,56]. Moreover, TiO$_2$ was used as support for
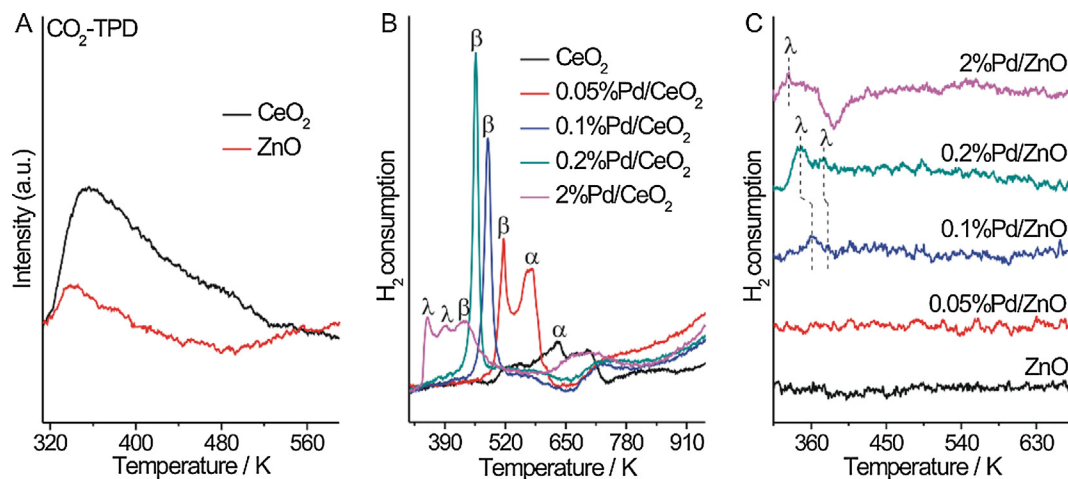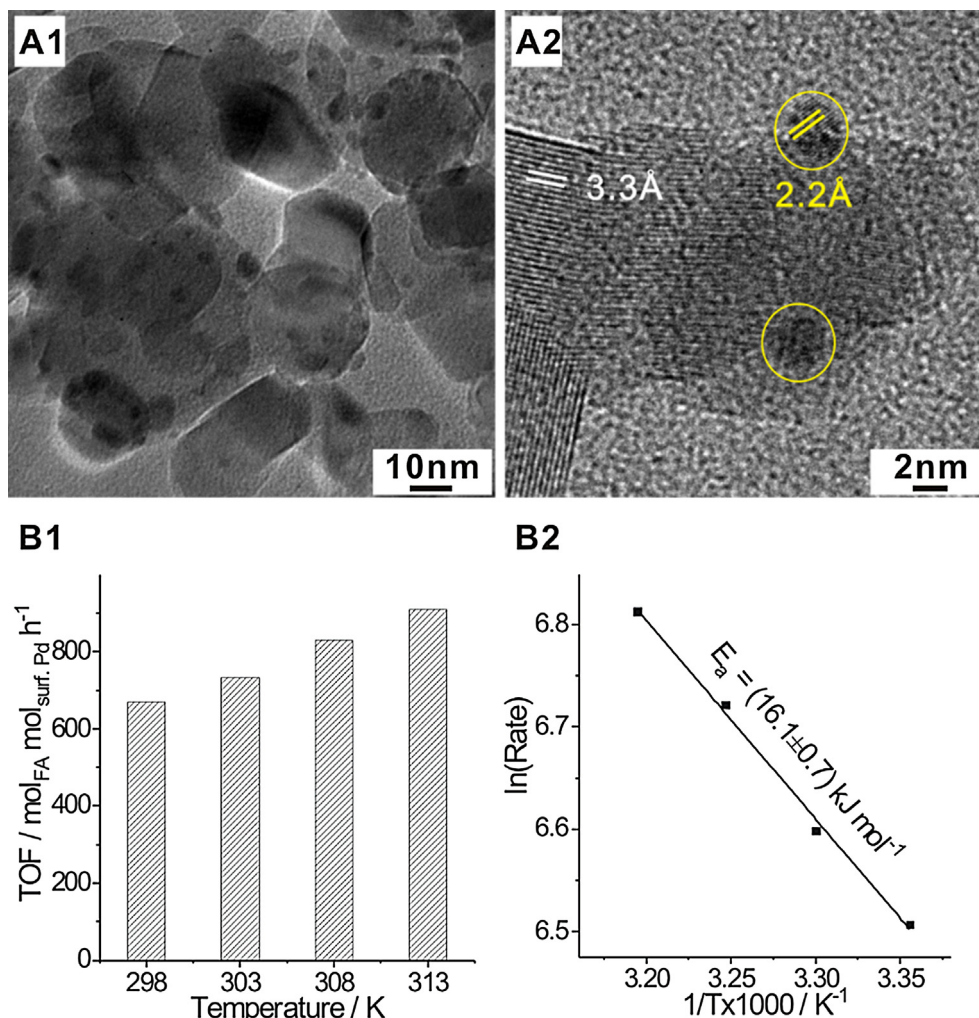

Fig. 7. (A) CO_2-TPD profiles of CeO$_2$ and ZnO; H_2-TPR profiles of (B) CeO$_2$ and different Pd/CeO$_2$ catalysts, and (C) ZnO and various Pd/ZnO catalysts.

Fig. 8. (A1) TEM and (A2) HRTEM images of 2%Pd/TiO$_2$ catalyst; (B1) TOFs (mol$_{FA}$ mol$_{surf. Pd}^{-1}$h^{-1}) for the production of FA calculated by surface Pd atoms on 2%Pd/TiO$_2$ catalyst at different temperatures and (B2) the corresponding Arrhenius plots. The lattice fringes of 3.3 and 2.2 Å (indicated in yellow and white), correspond to the spacing of TiO$_2${2 0 0} (JCPDS card number 21-1272) and Pd{1 1 1} (JCPDS card number 65-2867) crystal planes respectively.

highly active Ag-Pd alloy- and Au-based catalysts for FA formation [22,57]. Therefore, a commercial TiO$_2$ (P25)-supported Pd catalyst with a Pd weight loading of 2% (2%Pd/TiO$_2$) was synthesized. The actual Pd loading was measured to be 1.9 wt% using ICP-OES. The crystal structure is confirmed by XRD patterns (Fig. S14A) and the absence of Pd-related diffraction signals may be due to the small particle size and low weight loading. TEM images show the existence of Pd NPs with size distributions of 4.6 ± 0.9 nm (Fig. 8A1 and Fig. S15). The corresponding HRTEM images (Fig. 8A2) suggest the presence of metallic Pd{1 1 1} crystal planes indicated by lattice fringes of 2.2 Å. CO adsorption DRIFT spectra (Fig. S14B) also prove the formation of metallic Pd with the typical metallic Pd bound CO adsorption peaks [43]. As-synthesized 2%Pd/TiO$_2$ catalyst was applied for the hydrogenation reaction of CO$_2$ to FA and exhibits high activity under mild reaction conditions. The calculated TOF (Fig. 8B1) reached 670 h^{-1} at room temperature and increased to 909 h^{-1} at 313 K which is much higher than Pd/AC catalyst and belongs to the best reported TOF values under comparable reaction conditions [18]. The E$_a$, determined using Arrhenius plots, was 16.1 ± 0.7 kJ mol^{-1} (Fig. 8B2), which is even smaller than for 2%Pd/CeO$_2$ catalyst. The above results confirm that TiO$_2$ indeed serves as a better catalyst support for the hydrogenation of CO$_2$.

In this work, we used a series of CeO$_2$ and ZnO supported Pd catalysts for the hydrogenation of CO$_2$ to FA. We investigated the

reaction mechanism and the factors that govern the catalytic activity. Reaction of CO$_2$ with the support to form surface adsorbed bicarbonate species promoted by surface basic sites, followed by Pd catalyzed hydrogenation into formate appear to be a general pathway for all Pd catalysts studied. In this context, activation and reaction of CO$_2$ into surface carbonaceous species is the rate-determining step for supports without sufficient densities of basic sites such as ZnO, where the structure of Pd does not play a crucial role. On the other hand, on supports such as CeO$_2$ where the formation of surface adsorbed carbonate is facile, reaction of surface adsorbed intermediates with activated H is rate-determining, so that the structure of Pd becomes the activity-determining factor. This study generates a deeper insight into the catalytic mechanism for the CO$_2$ hydrogenation to FA over heterogeneous catalysts, offers understanding why a TiO$_2$-supported Pd catalyst exhibits higher activity, and potentially provides clues for the development of enhanced catalysts for CO$_2$ hydrogenation.

Acknowledgements

Appendix A. Supplementary material

Supplementary data to this article can be found online at https://doi.org/10.1016/j.jcat.2019.06.048.

References

[1] W. Wang, S. Wang, X. Ma, J. Gong, Recent advances in catalytic hydrogenation of carbon dioxide, Chem. Soc. Rev. 40 (2011) 3703–3727.

[2] A. Álvarez, A. Bansode, A. Urakawa, A.V. Bavykina, T.A. Wezendonk, M. Makkee, J. Gascon, F. Kapteijn, Challenges in the greener production of formates/formic acid, methanol, and DME by heterogeneously catalyzed CO$_2$ hydrogenation processes, Chem. Rev. 117 (2017) 9804–9838.

[3] A.W. Kleij, M. North, A. Urakawa, CO$_2$ catalysis, ChemSusChem 10 (2017) 1036–1038.

[4] N. Yan, K. Philippot, Transformation of CO$_2$ by using nanoscale metal catalysts: cases studies on the formation of formic acid and dimethylether, Curr. Opin. Chem. Eng. 20 (2018) 86–92.

[5] F.C.F. Marcos, J.M. Assaf, E.M. Assaf, CuFe and CuCo supported on pillared clay as catalysts for CO$_2$ hydrogenation into value-added products in one-step, Mol. Catal. 458 (2018) 297–306.

[6] L. Liu, F. Fan, M. Bai, F. Xue, X. Ma, Z. Jiang, T. Fang, Mechanistic study of methanol synthesis from CO$_2$ hydrogenation on Rh-doped Cu(111) surfaces, Mol. Catal. 466 (2019) 26–36.

[7] D. Mellmann, P. Sponholz, H. Junge, M. Beller, Formic acid as a hydrogen storage material – development of homogeneous catalysts for selective hydrogen release, Chem. Soc. Rev. 45 (2016) 3954–3988.

[8] A. Boddien, D. Mellmann, F. Gärtner, R. Jackstell, H. Junge, P.J. Dyson, G. Laurenczy, R. Ludwig, M. Beller, Efficient dehydrogenation of formic acid using an iron catalyst, Science 333 (2011) 1733–1736.

[9] A. Boddien, F. Gärtner, C. Federsel, P. Sponholz, D. Mellmann, R. Jackstell, H. Junge, M. Beller, CO$_2$-"Neutral" hydrogen storage based on bicarbonates and formates, Angew. Chem. Int. Ed. 50 (2011) 6411–6414.

[10] G.H. Gunasekar, K. Park, K.-D. Jung, S. Yoon, Recent developments in the catalytic hydrogenation of CO$_2$ to formic acid/formate using heterogeneous catalysts, Inorg. Chem. Front. 3 (2016) 882–895.

[11] G. Bredig, S.R. Carter, Katalytische synthese der ameisensäure unter druck, Ber. Dtsch. Chem. Ges. 47 (1914) 541–545.

[12] C. Hao, S. Wang, M. Li, L. Kang, X. Ma, Hydrogenation of CO$_2$ to formic acid on supported ruthenium catalysts, Catal. Today 160 (2011) 184–190.

[13] V. Srivastava, In situ generation of Ru nanoparticles to catalyze CO$_2$ hydrogenation to formic acid, Catal. Lett. 144 (2014) 1745–1750.

[14] T. Umegaki, Y. Enomoto, Y. Kojima, Metallic ruthenium nanoparticles for hydrogenation of supercritical carbon dioxide, Catal. Sci. Technol. 6 (2016) 409–412.

[15] K. Mori, T. Taga, H. Yamashita, Isolated single-atomic Ru catalyst bound on a layered double hydroxide for hydrogenation of CO$_2$ to formic acid, ACS Catal. 7 (2017) 3147–3151.

[16] D. Preti, S. Squarcialupi, G. Fachinetti, Conversion of syngas into formic acid, ChemCatChem 4 (2012) 469–471.

[17] C.J. Stalder, S. Chao, D.P. Summers, M.S. Wrighton, Supported palladium catalysts for the reduction of sodium bicarbonate to sodium formate in aqueous solution at room temperature and one atmosphere of hydrogen, J. Am. Chem. Soc. 105 (1983) 6318–6320.

[18] J. Su, L. Yang, M. Lu, H. Lin, Highly efficient hydrogen storage system based on ammonium bicarbonate/formate redox equilibrium over palladium nanocatalysts, ChemSusChem 8 (2015) 813–816.

[19] J. Su, M. Lu, H. Lin, High yield production of formate by hydrogenating CO$_2$ derived ammonium carbamate/carbonate at room temperature, Green Chem. 17 (2015) 2769–2773.

[20] Q.-Y. Bi, J.-D. Lin, Y.-M. Liu, X.-L. Du, J.-Q. Wang, H.-Y. He, Y. Cao, An Aqueous rechargeable formate-based hydrogen battery driven by heterogeneous Pd catalysis, Angew. Chem. Int. Ed. 53 (2014) 13583–13587.

[21] J.H. Lee, J. Ryu, J.Y. Kim, S.-W. Nam, J.H. Han, T.-H. Lim, S. Gautam, K.H. Chae, C. W. Yoon, Carbon dioxide mediated, reversible chemical hydrogen storage using a Pd nanocatalyst supported on mesoporous graphitic carbon nitride, J. Mater. Chem. A 2 (2014) 9490–9495.

[22] K. Mori, T. Sano, H. Kobayashi, H. Yamashita, Surface engineering of a supported PdAg catalyst for hydrogenation of CO$_2$ to formic acid: elucidating the active Pd atoms in alloy nanoparticles, J. Am. Chem. Soc. 140 (2018) 8902–8909.

[23] X. Lv, G. Lu, Z.-Q. Wang, Z.-N. Xu, G.-C. Guo, Computational evidence for lewis base-promoted CO$_2$ hydrogenation to formic acid on gold surfaces, ACS Catal. 7 (2017) 4519–4526.

[24] X. Yang, S. Kattel, S.D. Senanayake, J.A. Boscoboinik, X. Nie, J. Graciani, J.A. Rodriguez, P. Liu, D.J. Stacchiola, J.G. Chen, Low pressure CO$_2$ hydrogenation to

[25] methanol over gold nanoparticles activated on a CeO$_x$/TiO$_2$ interface, J. Am. Chem. Soc. 137 (2015) 10104–10107.

[25] Q. Liu, X. Yang, L. Li, S. Miao, Y. Li, Y. Li, X. Wang, Y. Huang, T. Zhang, Direct catalytic hydrogenation of CO$_2$ to formate over a Schiff-base-mediated gold nanocatalyst, Nat. Commun. 8 (2017) 1407.

[26] S. Masuda, K. Mori, Y. Futamura, H. Yamashita, PdAg nanoparticles supported on functionalized mesoporous carbon: promotional effect of surface amine groups in reversible hydrogen delivery/storage mediated by formic acid/CO$_2$, ACS Catal. 8 (2018) 2277–2285.

[27] W. Fanan, X. Jinming, S. Xianzhao, S. Xiong, H. Yanqiang, Z. Tao, Palladium on nitrogen-doped mesoporous carbon: a bifunctional catalyst for formate-based carbon-neutral hydrogen storage, ChemSusChem 9 (2016) 246–251.

[28] Q.-L. Zhu, N. Tsumori, Q. Xu, Immobilizing extremely catalytically active palladium nanoparticles to carbon nanospheres: a weakly-capping growth approach, J. Am. Chem. Soc. 137 (2015) 11743–11748.

[29] L.T.M. Nguyen, H. Park, M. Banu, J.Y. Kim, D.H. Youn, G. Magesh, W.Y. Kim, J.S. Lee, Catalytic CO$_2$ hydrogenation to formic acid over carbon nanotube-graphene supported PdNi alloy catalysts, RSC Adv. 5 (2015) 105560–105566.

[30] M.S. Maru, S. Ram, R.S. Shukla, N.-u.H. Khan, Ruthenium-hydrotalcite (Ru-HT) as an effective heterogeneous catalyst for the selective hydrogenation of CO$_2$ to formic acid, Mol. Catal. 446 (2018) 23–30.

[31] Z. Zhang, L. Zhang, M.J. Hülsey, N. Yan, Zirconia phase effect in Pd/ZrO$_2$ catalyzed CO$_2$ hydrogenation into formate, Mol. Catal. 475 (2019) 110461.

[32] H. Bahruji, M. Bowker, G. Hutchings, N. Dimitratos, P. Wells, E. Gibson, W. Jones, C. Brookes, D. Morgan, G. Lalev, Pd/ZnO catalysts for direct CO$_2$ hydrogenation to methanol, J. Catal. 343 (2016) 133–146.

[33] O. Martin, A.J. Martín, C. Mondelli, S. Mitchell, T.F. Segawa, R. Hauert, C. Drouilly, D. Curulla-Ferré, J. Pérez-Ramírez, Indium oxide as a superior catalyst for methanol synthesis by CO$_2$ hydrogenation, Angew. Chem. Int. Ed. 55 (2016) 6261–6265.

[34] J. Wang, G. Li, Z. Li, C. Tang, Z. Feng, H. An, H. Liu, T. Liu, C. Li, A highly selective and stable ZnO-ZrO$_2$ solid solution catalyst for CO$_2$ hydrogenation to methanol, Sci. Adv. 3 (2017) e1701290.

[35] G.A. Filonenko, W.L. Vrijburg, E.J.M. Hensen, E.A. Pidko, On the activity of supported Au catalysts in the liquid phase hydrogenation of CO$_2$ to formates, J. Catal. 343 (2016) 97–105.

[36] E.J. Choi, Y.H. Lee, D.-W. Lee, D.-J. Moon, K.-Y. Lee, Hydrogenation of CO$_2$ to methanol over Pd–Cu/CeO$_2$ catalysts, Mol. Catal. 434 (2017) 146–153.

[37] C. Tisseraud, C. Comminges, A. Habrioux, S. Pronier, Y. Pouilloux, A. Le Valant, Cu-ZnO catalysts for CO$_2$ hydrogenation to methanol: Morphology change induced by ZnO lixiviation and its impact on the active phase formation, Mol. Catal. 446 (2018) 98–105.

[38] A. Trovarelli, C. Deleitenburg, G. Dolcetti, J.L. Lorca, CO$_2$ methanation under transient and steady-state conditions over Rh/CeO$_2$ and CeO$_2$-promoted Rh/SiO$_2$: the role of surface and bulk ceria, J. Catal. 151 (1995) 111–124.

[39] W. Li, A. Wang, X. Liu, T. Zhang, Silica-supported Au–Cu alloy nanoparticles as an efficient catalyst for selective oxidation of alcohols, Appl. Catal., A (2012) 146–151.

[40] S.F.J. Hackett, R.M. Brydson, M.H. Gass, I. Harvey, A.D. Newman, K. Wilson, A.F. Lee, High-activity, single-site mesoporous Pd/Al$_2$O$_3$ catalysts for selective aerobic oxidation of allylic alcohols, Angew. Chem. Int. Ed. 46 (2007) 8593–8596.

[41] M.L. Cubeiro, J.L.G. Fierro, Selective production of hydrogen by partial oxidation of methanol over ZnO-supported palladium catalysts, J. Catal. 179 (1998) 150–162.

[42] K.R. Priolkar, P. Bera, P.R. Sarode, M.S. Hegde, S. Emura, R. Kumashiro, N.P. Lalla, Formation of Ce$_{1-x}$Pd$_x$O$_{2-\delta}$ solid solution in combustion-synthesized Pd/CeO$_2$ catalyst: XRD, XPS, and EXAFS investigation, Chem. Mater. 14 (2002) 2120–2128.

[43] H. Jeong, J. Bae, J.W. Han, H. Lee, Promoting effects of hydrothermal treatment on the activity and durability of Pd/CeO$_2$ catalysts for CO oxidation, ACS Catal. 7 (2017) 7097–7105.

[44] L. Meng, A.-P. Jia, J.-Q. Lu, L.-F. Luo, W.-X. Huang, M.-F. Luo, Synergetic effects of PdO species on CO oxidation over PdO–CeO$_2$ catalysts, J. Phys. Chem. C 115 (2011) 19789–19796.

[45] T. Das, G. Deo, Synthesis, characterization and in situ DRIFTS during the CO$_2$ hydrogenation reaction over supported cobalt catalysts, J. Mol. Catal. Chem. 350 (2011) 75–82.

[46] X. Wang, H. Shi, J.H. Kwak, J. Szanyi, Mechanism of CO$_2$ hydrogenation on Pd/Al$_2$O$_3$ catalysts: kinetics and transient DRIFTS-MS studies, ACS Catal. 5 (2015) 6337–6349.

[47] S. Chen, L. Luo, Z. Jiang, W. Huang, Size-dependent reaction pathways of low-temperature CO oxidation on Au/CeO$_2$ catalysts, ACS Catal. 5 (2015) 1653–1662.

[48] X. Wang, J.A. Rodriguez, J.C. Hanson, D. Gamarra, A. Martínez-Arias, M. Fernández-García, In situ studies of the active sites for the water gas shift reaction over Cu–CeO$_2$ catalysts: complex interaction between metallic copper and oxygen vacancies of ceria, J. Phys. Chem. C 110 (2006) 428–434.

[49] J.C.S. Wu, C.-W. Huang, In situ DRIFTS study of photocatalytic CO$_2$ reduction under UV irradiation, Front. Chem. Eng. Chin. 4 (2010) 120–126.

[50] P.A.U. Aldana, F. Ocampo, K. Kobl, B. Louis, F. Thibault-Starzyk, M. Daturi, P. Bazin, S. Thomas, A.C. Roger, Catalytic CO$_2$ valorization into CH$_4$ on Ni-based ceria-zirconia. reaction mechanism by operando IR spectroscopy, Catal. Today 215 (2013) 201–207.

[51] A. Álvarez, M. Borges, J.J. Corral-Pérez, J.G. Olcina, L. Hu, D. Cornu, R. Huang, D. Stoian, A. Urakawa, CO$_2$ activation over catalytic surfaces, ChemPhysChem 18 (2017) 3135–3141.

[52] H. Zhu, Z. Qin, W. Shan, W. Shen, J. Wang, Pd/CeO$_2$–TiO$_2$ catalyst for CO oxidation at low temperature: a TPR study with H$_2$ and CO as reducing agents, J. Catal. 225 (2004) 267–277.

[53] K. Sun, W. Lu, M. Wang, X. Xu, Characterization and catalytic performances of La doped Pd/CeO$_2$ catalysts for methanol decomposition, Appl. Catal., A 268 (2004) 107–113.

[54] A.S. Malik, S.F. Zaman, A.A. Al-Zahrani, M.A. Daous, H. Driss, L.A. Petrov, Development of highly selective PdZn/CeO$_2$ and Ca-doped PdZn/CeO$_2$ catalysts for methanol synthesis from CO$_2$ hydrogenation, Appl. Catal., A 560 (2018) 42–53.

[55] F. Lu, B. Jiang, J. Wang, Z. Huang, Z. Liao, Y. Yang, J. Zheng, Promotional effect of Ti doping on the ketonization of acetic acid over a CeO$_2$ catalyst, RSC Adv. 7 (2017) 22017–22026.

[56] Z. Fu, Y. Zhong, Y. Yu, L. Long, M. Xiao, D. Han, S. Wang, Y. Meng, TiO$_2$-Doped CeO$_2$ nanorod catalyst for direct conversion of CO$_2$ and CH$_3$OH to dimethyl carbonate: catalytic performance and kinetic study, ACS Omega 3 (2018) 198–207.

[57] D. Preti, C. Resta, S. Squarcialupi, G. Fachinetti, Carbon dioxide hydrogenation to formic acid by using a heterogeneous gold catalyst, Angew. Chem. Int. Ed. 50 (2011) 12551–12554.